Combination Analysis and Switching Method of a Cascaded H-Bridge Multilevel Inverter Based on Transformers With the Different Turns Ratio for Increasing the Voltage Level

June-Seok Lee, *Member, IEEE*, Hyun-Woo Sim, Juyong Kim, and Kyo-Beum Lee, *Senior Member, IEEE*

***Abstract*—This paper analyzes the combination in a cascaded H-bridge multilevel inverter (CHBI) based on transformers with the different turn ratios for increasing the voltage level and proposes the switching method for achieving the output voltage distribution among H-bridge cells (HBCs). The transformers used in this paper are connected to the output of the respective HBCs, and the secondary sides of all the transformers are connected in series for generating the final output voltage. Only one of the transformers, in particular, has a different turn ratio for increasing the output voltage level. In this paper, the possible turn ratio of the special transformer with a different turn ratio is discussed in detail, and a switching method based on the level-shifted switching method for the topology used in this paper is proposed. To verify the effectiveness of the proposed method, a three-phase 21-level CHBI is experimentally tested.**

***Index Terms*—Cascaded H-bridge inverter (CHBI), cascaded multilevel, level-shifted switching method, multilevel inverter.**

I. Introduction

RESEARCH on multilevel inverters used in high-power and voltage applications are being conducted because of the recent increase in system power requirements. Owing to many advantages compared to conventional two-level inverters [1], [2], multilevel inverters are used in various high-power and voltage applications such as wind turbine systems [3], [4], grid connected systems [5]–[7], and motor drive systems [8], [9].

There are several multilevel inverter topologies: the neutral-point clamped topology [2], [4], [7], the flying capacitor topology [10], [11], the cascaded H-bridge (CHB) topology [3], [6], etc., [5], [8], [9]. Each topology has its own advantages. Among them, the effective topology for high-voltage applications is the CHB topology having a degree of freedom for increasing the voltage level by connecting H-bridge cells (HBCs) in series with simplicity in control.

The traditional CHB topology consists of several HBCs with their outputs connected in series. A main drawback of the topology is that the input sources (dc side) of the HBCs should be isolated from each other. Therefore, low frequency transformers with rectifiers are used to supply the isolated source [12]. Although the number of transformer can be reduced by a specially designed multiphase transformer [1], [13], the remaining rectifiers continue to be a drawback, and the multiphase transformer nullifies the advantage of the degree of freedom in increasing the voltage level.

To overcome the problems mentioned above, two concepts have been studied: the topologies using the floating capacitors [14]–[16] and new topologies with transformers and the single dc source [17]–[21]. The former topologies have the complex structure and its control method is complex in order to regulate the floating capacitor voltage. In the latter topologies, the main difference is that transformers are connected to the outputs of the HBCs. CHB topologies using output transformers have lesser switching components than the traditional CHB topologies with transformers and rectifiers, thereby relatively retaining the degree of freedom in increasing the voltage level. In addition, a high voltage level can be achieved using transformers with different turns ratios [20]. Based on these advantages, research on the multilevel topology with the output transformers and single dc-link have continued consistently, although it has a disadvantage in terms of tolerant operation when the subsystem of input side breaks down.

The each HBC generates the one-pulse in its output voltage during the half of the fundamental period and they are combined to achieve the sinusoidal output voltage in [19]. The new

Manuscript received December 6, 2016; revised March 29, 2017, June 23, 2017, August 24, 2017, and October 9, 2017; accepted October 16, 2017. Date of publication November 13, 2017; date of current version February 13, 2018. This work was supported in part by a grant from R&D Program of the Korea Railroad Research Institute, Republic of Korea, and in part by Basic Science Research Program through the National Research Foundation of Korea (NRF) funded by the Ministry of Science, ICT & Future Planning (2016R1A2B4010636). *(Corresponding author: Kyo-Beum Lee.)*

J.-S. Lee is with the Railroad Safety Research Division, Korea Railroad Research Institute, Uiwang 16105, South Korea (e-mail: ljs@krri.re.kr).

H.-W. Sim is with the Electric Energy Engineering Team of Hyundai Mobis, Yongin 16891, South Korea (e-mail: hw.sim@mobis.co.kr).

J. Kim is with the Korea Electric Power Corporation, Naju 58217, South Korea (e-mail: juyong.kim@kepco.co.kr).

K.-B. Lee is with the Department of Electrical and Computer Engineering, Ajou University, Suwon 16499, South Korea (e-mail: kyl@ajou.ac.kr).

Color versions of one or more of the figures in this paper are available online at http://ieeexplore.ieee.org.

Digital Object Identifier 10.1109/TIE.2017.2772139

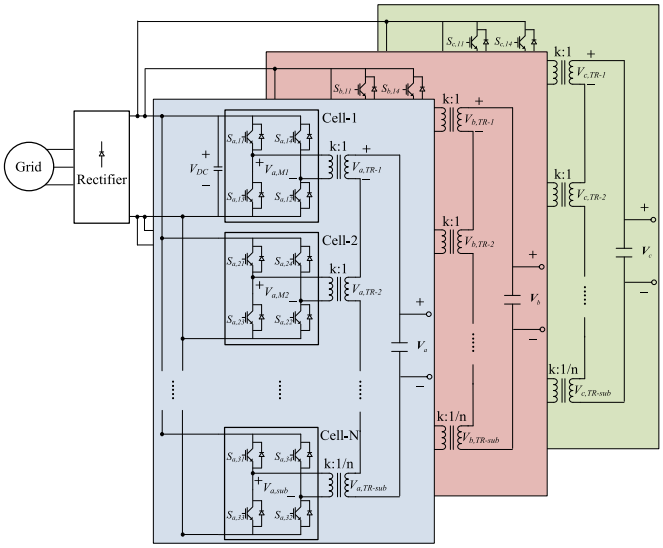

Fig. 1. Transformer-based CHBI topology used in this paper.

switching pattern, which is based on the ON/OFF angle, depending on the modulation index is proposed in [18], and it guarantees the balanced output voltage and power. The 27-level CHB inverter (CHBI) is a representative topology [20]. In this topology, three HBCs per phase are used. Although three HBCs can generate an output voltage with 7-levels in the traditional CHBI topology, connecting the output of each HBC to three transformers with turns ratios of k:1, k:1/3, and k:1/9, respectively, extends the voltage level from 7 to 21. In a 27-level CHBI, each HBC shows a different switching operation. A HBC connected to a transformer with a k:1 turns ratio (main transformer) operates at a low switching frequency; however, a HBC connected to a transformer with a k:1/9 turns ratio operates at a high switching frequency. In terms of the power distribution, the HBC with the main transformer takes charge of a significant part of the total power. The power of other HBCs is reduced according to the decrease in the turns ratios of the transformers. Consequently, each HBC should be designed independently, considering its power rate, which means that the effort for developing the transformer is required, and the total cost can be increased.

A transformer-based CHBI topology which has the different configuration with [18]–[20] is introduced and considered in this paper. The transformer-based CHBI topology can use several main transformers with k:1 turns ratios and one subtransformer with k:$1/n$ ($n = 2, 3$), as shown in Fig. 1. Most of the power can be divided by the HBCs (main HBC, MHBC) connected to the main transformer; they can comply with the same design rule. The HBC (subHBC, SHBC) connected to the subtransformer takes charge of a small portion of the total power. The feasibility of the configuration of the transformer-based CHBI topology is analyzed by applying the proposed switching method. Finally, the effectiveness of the proposed switching method is verified experimentally in the transformer-based 21-level CHBI.

II. Configuration Analysis of the Transformer-Based CHBI Topology

The transformer-based CHBI topology used in this paper is shown in Fig. 1. A rectifier is used to transform the ac voltages of the grid to the dc voltage of the dc link and all the HBCs share the dc link, i.e., they are connected to the dc link in parallel. The most important characteristic of this topology is that each H-bride cell has a transformer at its output. One HBC, called the SHBC, has a special transformer that is different from the others. Several HBCs, called MHBCs, use the same transformer and are in charge of the most of power transmission. Depending on the number of MHBCs, the feasible maximum (minimum) voltage is defined and the voltage level that can be calculated by a basic voltage level calculation equation for the traditional CHBI topology is determined [21]. In the transformer-based CHBI topology, the final output voltage $(V_x, x = a, b, c)$ is generated by synthesizing the output voltages $(V_{x,\mathrm{TR}-M}, x = a, b, c, M = 1, 2, \ldots, N-1,)$ of the main transformers (TR-main) and the output voltage $(V_{x,\mathrm{TR}-\mathrm{sub}}, \mathrm{x} = a, b, c)$ of the special transformer (TR-sub). Therefore, the voltage level is divided further using the TR-Sub and the feasible value of V_x is expressed as

$$V_x = \pm\tfrac{V_{\mathrm{DC}}}{k}M \pm \tfrac{V_{\mathrm{DC}}}{kn}S \begin{matrix} M = 0, 1, \ldots, N-1 \\ S = 0, 1 \end{matrix} \tag{1}$$

where N is the number of HBCs ($N-1$ indicates the number of MHBCs), S is the number of SHBCs, k is the primary side turns ratio constant for all the transformers used in the transformer-based CHBI topology, and n is the secondary side turns ratio constant of the TR-sub connected to the SHBC.

The minimum variation (dV_x) of the voltage level is determined by the TR-sub and is expressed as

$$dV_x = \frac{V_{\mathrm{DC}}}{kn}. \tag{2}$$

In the transformer-based CHBI topology, the number of voltage level is calculated as

$$2 \times \frac{V_{x,\max}}{\frac{V_{\mathrm{DC}}}{kn}} + 1 = 2n(N-1) + 3,$$

$$V_{x,\max} = \frac{V_{\mathrm{DC}}(N-1)}{k} + \frac{V_{\mathrm{DC}}}{kn}. \tag{3}$$

The number of voltage level is not influenced by k. To identify a feasible configuration for the transformer-based CHBI topology, the parameters (n, N) should be reviewed, excluding the case where $n = 1$ because it indicates a traditional CHBI topology using N-HBCs. Assuming that $n = 2$, the value of V_x is calculated as

$$V_x = V_{x,\mathrm{TM}-1} + \cdots + V_{x,\mathrm{TM}-M} + V_{x,\mathrm{TM}-sub}\ x = a, b, c$$

$$V_{x,\mathrm{TM}-M} = -\frac{V_{\mathrm{DC}}}{k}, 0, \frac{V_{\mathrm{DC}}}{k} \quad M = 1, 2, \ldots, (N-1)$$

$$V_{x,\mathrm{TM}-\mathrm{sub}} = -\frac{V_{\mathrm{DC}}}{2k}, 0, \frac{V_{\mathrm{DC}}}{2k}. \tag{4}$$

The result of (4), where $N = 2$ or 3 is summarized in Table I. Hence, when using the TR-sub with a turns ratio of k : 1/2, the number of MHBCs can be increased without any limitation, implying that dV_x is always the same. In addition, a TR-sub with turns ratio of k : 1/3 is acceptable in the transformer-based CHBI topology. In the other case, where $n > 3$, V_x cannot acquire all the values of the voltage levels shown in Table II.

TABLE I
FEASIBLE VALUES OF V_x DEPENDING ON n, WHEN n IS 2

(*N*-1)	$V_{x,TR-M}$s	$V_{x,TR-sub}$	V_x ($V_{DC}/2k=dV_x$)	Levels
1	V_{DC}/k 0 $-V_{DC}/k$	$V_{DC}/2k$ 0 $-V_{DC}/2k$	$3dV_x$, $2dV_x$, dV_x dV_x, 0, $-dV_x$ $-dV_x$, $-2dV_x$, $-3dV_x$	9-level ($3dV_x \sim -3dV_x$)
2	$2V_{DC}/k$ V_{DC}/k 0 $-V_{DC}/k$ $-2V_{DC}/k$		$5dV_x$, $4dV_x$, $3dV_x$ $3dV_x$, $2dV_x$, dV_x dV_x, 0, $-dV_x$ $-dV_x$, $-2dV_x$, $-3dV_x$ $-3dV_x$, $-4dV_x$, $-5dV_x$	15-level ($5dV_x \sim -5dV_x$)

TABLE II
FEASIBLE VALUES OF V_x WHEN n IS 4

(*N*-1)	$V_{x,TR-M}$s	$V_{x,TR-sub}$	V_x ($V_{DC}/4k=dV_x$)	Levels
1	V_{DC}/k 0 $-V_{DC}/k$	$V_{DC}/4k$ 0 $-V_{DC}/4k$	$5dV_x$, $4dV_x$, $3dV_x$ dV_x, 0, $-dV_x$ $-3dV_x$, $-4dV_x$, $-5dV_x$	9-level (Not equal)

TABLE III
VOLTAGE LEVEL OF V_x DEPENDING ON N AND n

Number of HBCs (*N*)	Traditional *n* = 1 (*k*:1/1)	Transformer-based CHBI used in this paper *n* = 2 (*k*:1/2)	*n* = 3 (*k*:1/3)
2	5	7	9
3	7	11	15
4	9	15	21
N	2*N*+1 [17]	4*N*-1	6*N*-3

Although the voltage level is nine, dV_x is not always the same because TR-sub with a turns ratio of k : 1/4 cannot generate $2dV_x$ and $-2dV_x$. Although the absence of the voltage levels, $2dV_x$ and $-2dV_x$, is not an issue for generating a linear output voltage, this configuration cannot be guaranteed by the proposed switching method introduced in Section III.

In the transformer-based CHBI topology, dV_x of the voltage level is determined only by n and the voltage level is defined depending on both N and n. Table III shows the feasible voltage levels, depending on N and n. As the number of MHBCs used increases, the benefit in terms of the voltage level also increases.

III. PROPOSED SWITCHING METHOD

To generate the maximum output voltage level of the transformer-based CHBI topology, the switching method is needed. In introducing the switching method based on carrier signals, a 21-level CHBI using four HBCs (three MHBCs and an SHBC connected to a TR-sub with k : 1/3 ($n = 3$)) is used.

A. Output Voltage Determination

A HBC has a three-level output voltage: $V_{\mathrm{DC}}, 0, -V_{\mathrm{DC}}$. Considering the TRs' output voltages ($V_{x,\mathrm{TR-MS}}$,$V_{x,\mathrm{TR-sub}}$), the basic voltage level becomes dV_x. The positive values of V_x can be expressed as shown in Table IV. Among the voltage levels of V_x, the voltage levels from $2dV_x$ to $7dV_x$ can be generated by three combinations. Therefore, the switching method for the transformer-based CHBI topology is based on the level-shifted switching method [1], [21]–[23], [26].

B. Switching Method Based on Carrier Signals

As the number of HBCs increase, more carrier signals are required in the level-shifted switching method. An m-level CHBI requires (m–1) carrier signals. Two carrier signals are needed for a HBC and each carrier signal operates one leg of the HBC, respectively. In real systems using microcontrollers, the reference voltage (V_{ref}) that is compared to the several carrier signals for operating the switches of the HBC is changed to use one carrier signal.

Similar to the existing carrier-based level shifted switching methods, the switching method for the transformer-based CHBI topology needs (output voltage level-1) carrier signals. Twenty carrier signals are used in the 21-level CHBI and each carrier signal takes charge of a leg of the HBCs. However, in real system, only two types (V_{c1}, V_{c2}) of carrier signals are used and the reference voltages ($V_{x,\mathrm{ref},yA}, V_{x,\mathrm{ref},yB}$, y = 1, 2, 3, S) for the MHBCs and SBHC are obtained from the x-phase reference voltage ($V_{x,\mathrm{ref}}$). The operating principle of the switching method is based on the characteristic of Table IV.

Fig. 2 shows the switching operation in the MHBCs. Two phase-shifted carrier signals (V_{c1}, V_{c2}) and six reference voltages ($V_{x,\mathrm{ref},yA}, V_{x,\mathrm{ref},yB}, y = 1, 2, 3$) for each leg (−A, −B) of the three MHBCs in the x-phase are used. V_{c1} is compared to $V_{x,\mathrm{ref},1A}$, $V_{x,\mathrm{ref},2A}$, and $V_{x,\mathrm{ref},3A}$ that are obtained from the positive V_{ref} and are used to operate the switches in the A-leg of each MHBC. V_{c2} is used to operate the switches in the B-leg. In case of $V_{x,\mathrm{ref},1A}$, $V_{x,\mathrm{ref},1A} = 0$ when $V_{x,\mathrm{ref}} < 2\mathrm{dV_x}$, and $V_{x,\mathrm{ref},1A} = dV_x$ when $V_{x,\mathrm{ref}} > 3dV_x$; $V_{x,\mathrm{ref},1A}$ has a variable value when $V_{x,\mathrm{ref}}$ is in the range between $1dV_x$ and $2dV_x$ and it causes a switching operation during the range identified in the boxes of Table IV. The reference voltages for the MHBCs are generated by the rule of Table IV, and they are calculated as

if $V_{x,\mathrm{ref}} \geq 0$,

$$\begin{cases} V_{x,\mathrm{ref},1A} \\ = \begin{cases} 0 & \text{for } R_x = 1 \\ V_{x,\mathrm{ref}} - 1dV_x, & \text{for } R_x = 2 \\ dV_x & \text{for } R_x = 3, \ldots, 10 \end{cases}, V_{x,\mathrm{ref},1B} = 0 \\ V_{x,\mathrm{ref},2A} \\ = \begin{cases} 0 & \text{for } R_x = 1, \ldots, 4 \\ V_{x,\mathrm{ref}} - 4dV_x, & \text{for } R_x = 5 \\ dV_x & \text{for } R_x = 6, \ldots, 10 \end{cases}, V_{x,\mathrm{ref},2B} = 0 \\ V_{x,\mathrm{ref},3A} \\ = \begin{cases} 0 & \text{for } R_x = 1, \ldots, 7 \\ V_{x,\mathrm{ref}} - 7dV_x, & \text{for } R_x = 8 \\ dV_x & \text{for } R_x = 9, 10 \end{cases}, V_{x,\mathrm{ref},3B} = 0 \end{cases}$$

TABLE IV
OUTPUT VOLTAGE OF EACH HBC AND V_x ($V_{\mathrm{DC}}/3k = dV_x$)

V_x	$V_{x,\mathrm{TR}-1}$ of MHBC-1	$V_{x,\mathrm{TR}-2}$ of MHBC-2	$V_{x,\mathrm{TR}-3}$ of MHBC-3	$V_{x,\mathrm{TR}-\mathrm{sub}}$ of SHBC
$10dV_x$	$3\boldsymbol{dV}_x$	$3\boldsymbol{dV}x$	$3\boldsymbol{dV}_x$	$\boldsymbol{dV}_x$
$9dV_x$	$3\boldsymbol{dV}_x$	$3\boldsymbol{dV}x$	$3\boldsymbol{dV}_x$	$\mathbf{0}$
$8dV_x$	$3\boldsymbol{dV}_x$	$3\boldsymbol{dV}x$	$3\boldsymbol{dV}_x$	$-\boldsymbol{dV}_x$
$7dV_x$	$3\boldsymbol{dV}_x, (0), [3dV_x]$	$3\boldsymbol{dV}x, (3dV_x), [0]$	$\mathbf{0}, (3dV_x), [3dV_x]$	$\boldsymbol{dV}_x$
$6dV_x$	$3\boldsymbol{dV}_x, (0), [3dV_x]$	$3\boldsymbol{dV}x, (3dV_x), [0]$	$\mathbf{0}, (3dV_x), [3dV_x]$	$\mathbf{0}$
$5dV_x$	$3\boldsymbol{dV}_x, (0), [3dV_x]$	$3\boldsymbol{dV}x, (3dV_x), [0]$	$\mathbf{0}, (3dV_x), [3dV_x]$	$-\boldsymbol{dV}_x$
$4dV_x$	$3\boldsymbol{dV}_x, (0), [0]$	$\mathbf{0}, (3dVx), [0]$	$\mathbf{0}, (0), [3dV_x]$	$\boldsymbol{dV}_x$
$3dV_x$	$3\boldsymbol{dV}_x, (0), [0]$	$\mathbf{0}, (3dV_x), [0]$	$\mathbf{0}, (0), [3dV_x]$	$\mathbf{0}$
$2dV_x$	$3\boldsymbol{dV}_x, (0), [0]$	$\mathbf{0}, (3dV_x), [0]$	$\mathbf{0}, (0), [3dV_x]$	$-\boldsymbol{dV}_x$
$1dV_x$	$\mathbf{0}$	$\mathbf{0}$	$\mathbf{0}$	$\boldsymbol{dV}_x$
0	$\mathbf{0}$	$\mathbf{0}$	$\mathbf{0}$	$\mathbf{0}$

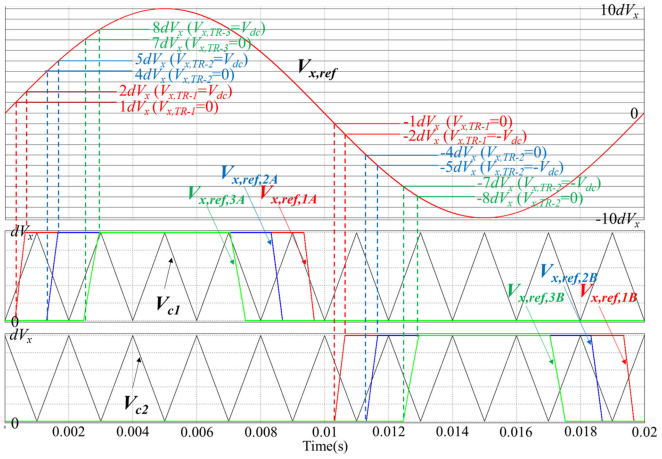

Fig. 2. Carrier signals (V_{c1} and V_{c2}) and reference voltages ($V_{x,\mathrm{ref},1A}, V_{x,\mathrm{ref},1B}, V_{x,\mathrm{ref},2A}, V_{x,\mathrm{ref},2B}, V_{x,\mathrm{ref},3A}, V_{x,\mathrm{ref},3B}$) for the switching operation in the MHBCs.

$$
\text{if} \quad V_{x,\mathrm{ref}} < 0,
$$

$$
\begin{cases}
V_{x,\mathrm{ref},1A} = 0, \\
V_{x,\mathrm{ref},1B} = \begin{cases} 0 & \text{for } R_x = 1 \\ V_{x,\mathrm{ref}} + 1dV_x, & \text{for } R_x = 2 \\ V_{\mathrm{dc}} & \text{for } R_x = 3, \ldots, 10 \end{cases} \\
V_{x,\mathrm{ref},2A} = 0, \\
V_{x,\mathrm{ref},2B} = \begin{cases} 0 & \text{for } R_x = 1, \ldots, 4 \\ V_{x,\mathrm{ref}} + 4dV_x, & \text{for } R_x = 5 \\ V_{\mathrm{dc}} & \text{for } R_x = 6, \ldots, 10 \end{cases} \\
V_{x,\mathrm{ref},3A} = 0, \\
V_{x,\mathrm{ref},2B} = \begin{cases} 0 & \text{for } R_x = 1, \ldots, 7 \\ V_{x,\mathrm{ref}} + 7dV_x, & \text{for } R_x = 8 \\ V_{\mathrm{dc}} & \text{for } R_x = 9, 10 \end{cases}
\end{cases} \tag{5}
$$

where R_x is the region including $V_{x,\mathrm{ref}}$ and is defined in Table V. The reference voltages for the HMBCs are 0 or dV_x for a considerable duration in one fundamental period of $V_{x,\mathrm{ref}}$ and the HMBCs have a smaller duration for the switching operation. Therefore, the HMBCs operate similar to a HBC applying the level-shifted switching method.

TABLE V
REGION OF THE REFERENCE VOLTAGE ($V_{x,\mathrm{ref}}$)

Voltage range	Region (R_x)
$0 < V_{x,ref} < 1dV_x$ or $-1dV_x < V_{x,ref} < 0$	1
$1dV_x < V_{x,ref} < 2dV_x$ or $-2dV_x < V_{x,ref} < -1dV_x$	2
$2dV_x < V_{x,ref} < 3dV_x$ or $-3dV_x < V_{x,ref} < -2dV_x$	3
$3dV_x < V_{x,ref} < 4dV_x$ or $-4dV_x < V_{x,ref} < -3dV_x$	4
$4dV_x < V_{x,ref} < 5dV_x$ or $-5dV_x < V_{x,ref} < -4dV_x$	5
$5dV_x < V_{x,ref} < 6dV_x$ or $-6dV_x < V_{x,ref} < -5dV_x$	6
$6dV_x < V_{x,ref} < 7dV_x$ or $-7dV_x < V_{x,ref} < -6dV_x$	7
$7dV_x < V_{x,ref} < 8dV_x$ or $-8dV_x < V_{x,ref} < -7dV_x$	8
$8dV_x < V_{x,ref} < 9dV_x$ or $-9dV_x < V_{x,ref} < -8dV_x$	9
$9dV_x < V_{x,ref} < 10dV_x$ or $-10dV_x < V_{x,ref} < -9dV_x$	10

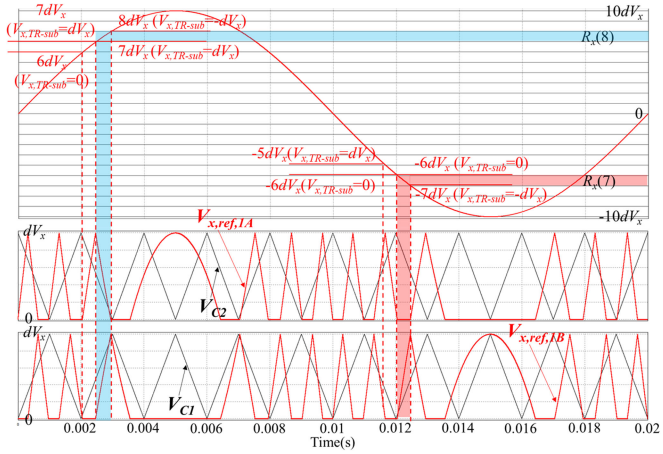

Fig. 3. Carrier signals (V_{c1} and V_{c2}) and reference voltages ($V_{x,\mathrm{ref},SA}, V_{x,\mathrm{ref},SB}$) for the switching operation of the SHBC.

The SHBC operation should divide V_x's voltage level further. This is achieved by complying with the rule in Table IV. Fig. 3 shows V_{c1}, V_{c2}, and the reference voltages ($V_{x,\mathrm{ref},SA}, V_{x,\mathrm{ref},SB}$) for the SHBC. The difference from the case of Fig. 2 is that V_{c1}

is compared to the B-leg reference voltage, $V_{x,\mathrm{ref,SB}}$; V_{c2} is used for operating the switches in the A-leg. In addition, $V_{x,\mathrm{ref},SA}$ and $V_{x,\mathrm{ref,SB}}$ of Fig. 3 are not simple. This is because the SHBC should operate like a HBC with a unipolar switching method or a bipolar switching method [28], depending upon the polarity of $V_{x,\mathrm{ref}}$ and R_x. In the shaded portion with the positive $V_{x,\mathrm{ref}}$ and $R_x(8)$ in Fig. 3, the bipolar switching method should be applied to the SHBC to result in an output voltage of either $-dV_x$ or dV_x. Therefore, $V_{x,\mathrm{ref},SA}$ and $V_{x,\mathrm{ref,SB}}$ have a variable value here. However, in the opposite side, in the shaded part with the negative $V_{x,\mathrm{ref}}$ and $R_x(7)$, the output voltage is defined as dV_x or 0 in Table IV. This implies that a unipolar switching method should be applied. In this region $V_{x,\mathrm{ref},SA}=0$, and only $V_{x,\mathrm{ref,SB}}$ has a valid value.

$V_{x,\mathrm{ref},SA}$ and $V_{x,\mathrm{ref,SB}}$ can be calculated using $V_{x,\mathrm{ref}}$ and R_x. It is expressed as

$$\text{if } V_{x,\mathrm{ref}} \geq 0,$$

$$\begin{cases} V_{x,\mathrm{ref},SA} \\ = \begin{cases} |V_{x,\mathrm{ref}}| - dV_x(R_x-1) & \text{for } R_x = 1,4,7,10 \\ dV_x - (|V_{x,\mathrm{ref}}| - dV_x(R_x-1)), & \text{for } R_x = 2,5,8 \\ 0 & \text{for } R_x = 3,6,9 \end{cases} \\ V_{x,\mathrm{ref},SB} \\ = \begin{cases} 0 & \text{for } R_x = 1,4,7,10 \\ |V_{x,\mathrm{ref}}| - dV_x(R_x-1), & \text{for } R_x = 2,5,8 \\ dV_x - (|V_{x,\mathrm{ref}}| - dV_x(R_x-1)) & \text{for } R_x = 3,6,9 \end{cases} \end{cases}$$

$$\text{if } V_{x,\mathrm{ref}} < 0,$$

$$\begin{cases} V_{x,\mathrm{ref},SA} \\ = \begin{cases} 0 & \text{for } R_x = 1,4,7,10 \\ |V_{x,\mathrm{ref}}| - dV_x(R_x-1), & \text{for } R_x = 2,5,8 \\ dV_x - (|V_{x,\mathrm{ref}}| - dV_x(R_x-1)) & \text{for } R_x = 3,6,9 \end{cases} \\ V_{x,\mathrm{ref},SB} \\ = \begin{cases} |V_{x,\mathrm{ref}}| - dV_x(R_x-1) & \text{for } R_x = 1,4,7,10 \\ dV_x - (|V_{x,\mathrm{ref}}| - dV_x(R_x-1)), & \text{for } R_x = 2,5,8 \\ 0 & \text{for } R_x = 3,6,9. \end{cases} \end{cases} \tag{6}$$

C. Balanced Voltage Distribution

The carrier-based switching method introduced in Section III-B for the transformer-based 21-level CHBI guarantees an output voltage with 21-levels; however, the voltage distribution in the three MHBCs is not considered. In Fig. 2, it is shown that the durations where $V_{x,\mathrm{ref},yA}$ or $V_{x,\mathrm{ref},yB}$, $y=1, 2, 3$ is dV_x are different. MHBC-1 has the longest time duration followed by MHBC-1, MHBC-2, and MHBC-3. In the transformer-based CHBI topology, an unbalanced voltage distribution leads to unbalanced power among the MHBCs and can result in different life times for each HBC because of the influence of the operating temperature on the aging process [24], [25]. This problem exists in CHBIs using the level-shifted switching method [26], [27].

TABLE VI
OUTPUT VOLTAGE OF EACH HBC AND V_x ($V_{\mathrm{DC}}/3k = dV_x$)

V_x	$V_{x,TR\text{-}1}$ of MHBC-1	$V_{x,TR\text{-}2}$ of MHBC-2	$V_{x,TR\text{-}3}$ of MHBC-3	$V_{x,TR\text{-}sub}$ of SHBC	R_x	$R_{x,old}$
0	0	0	0	0	R_1	
$1dV_x$	0	0	0	dV_x	R_2	R_1
$2dV_x$	0	0	$3dV_x$	$-dV_x$	R_3	
$3dV_x$	0	0	$3dV_x$	0	R_4	
$4dV_x$	0	0	$3dV_x$	dV_x	R_5	R_4
$5dV_x$	0	$3dV_x$	$3dV_x$	$-dV_x$	R_6	
$6dV_x$	0	$3dV_x$	$3dV_x$	0	R_7	
$7dV_x$	0	$3dV_x$	$3dV_x$	dV_x	R_8	R_7
$8dV_x$	$3dV_x$	$3dV_x$	$3dV_x$	$-dV_x$	R_9	
$9dV_x$	$3dV_x$	$3dV_x$	$3dV_x$	0		
$10dV_x$	$3dV_x$	$3dV_x$	$3dV_x$	dV_x	R_{10}	
$9dV_x$	$3dV_x$	$3dV_x$	$3dV_x$	0	R_9	
$8dV_x$	$3dV_x$	$3dV_x$	$3dV_x$	$-dV_x$	R_8	R_9
$7dV_x$	$3dV_x$	$3dV_x$	0	dV_x	R_7	
$6dV_x$	$3dV_x$	$3dV_x$	0	0	R_6	
$5dV_x$	$3dV_x$	$3dV_x$	0	$-dV_x$	R_5	R_6
$4dV_x$	$3dV_x$	0	0	dV_x	R_4	
$3dV_x$	$3dV_x$	0	0	0	R_3	
$2dV_x$	$3dV_x$	0	0	$-dV_x$	R_2	R_3
$1dV_x$	0	0	0	dV_x	R_1	
0	0	0	0	0		

To improve the unbalanced voltage distribution, Table IV should be changed to Table VI. In the 21-level CHBI topology, a balanced voltage distribution for the three MHBCs is achieved in one-half of the fundamental period and the key equations are represented as

$$V_{M1} = |V_{x,\mathrm{ref}}| - (R_x - 1)dV_x \tag{7}$$

$$V_{M2} = dV_x - (|V_{x,\mathrm{ref}}| - (R_x - 1)dV_x). \tag{8}$$

Using (7) and (8), all the reference voltages can be summarized as shown in Table VII. $R_{x,\mathrm{old}}$ is the old value of R_x. $R_{x,\mathrm{old}}$ is used to distinguish the different output states of the MHBCs in regions such as $R_x(2)$, $R_x(5)$, and $R_x(8)$ and is defined for the range, $R_x(2) -_x (8)$. For instance, in the case of $R_x(8)$, when $R_{x,\mathrm{old}}=7$, MHBC-1 switches the output voltage to $3dV_x$ or 0 and the MHBC-2 and MHBC-3 have an output voltage of only $3dV_x$. On the other hand, only the MHBC-3 switches the output voltage to $3dV_x$ or 0, when $R_{x,\mathrm{old}}=9$.

D. Balanced Power Distribution

In the previous section, a balanced power distribution was achieved by regenerating the reference voltages. However, the transmitted power of each HBC is not balanced yet because it is determined by the current (I_x) as well as by the voltage of the HBC. The three voltages $(V_{x,\mathrm{TR}-y},\ y=1, 2, 3)$ of the MHBCs have the same I_x as shown in Fig. 4(a). The transmitted power that is the multiplication of the current and voltage is represented as area of the current, when an output voltage exists in the MHBC. Although the power is delivered through the three MHBCs, the power balance is not achieved in MHBCs as shown in colored areas of Fig. 4(a). As a solution to this problem, the HBC rotating method [21], [26], [28] used in the level-shifted switching method is applied in this paper, as shown in Fig. 4(b).

TABLE VII

REFERENCE VOLTAGES FOR THE TRANSFORMER-BASED 21-LEVEL CHBI TOPOLOGY, WHEN $V_{x,\mathrm{ref}}$ IS POSITIVE ([] INDICATES THAT $V_{x,\mathrm{ref}}$ IS NEGATIVE)

R_x-$R_{x,old}$	$V_{x,ref,1A}$	$V_{x,ref,1B}$	$V_{x,ref,2A}$	$V_{x,ref,2B}$	$V_{x,ref,3A}$	$V_{x,ref,3B}$	$V_{x,ref,SA}$	$V_{x,ref,SB}$
1	0 [0]	0 [0]	0 [0]	0 [0]	0 [0]	0 [0]	V_{M1} [0]	0 [V_{M1}]
2-1	0 [0]	0 [0]	0 [0]	0 [0]	V_{M1} [0]	0 [V_{M1}]	V_{M2} [V_{M1}]	V_{M1} [V_{M2}]
3-2	0 [0]	0 [0]	0 [0]	0 [0]	dV_x [0]	0 [dV_x]	0 [V_{M2}]	V_{M2} [0]
4-3	0 [0]	0 [0]	0 [0]	0 [0]	dV_x [0]	0 [dV_x]	V_{M1} [0]	0 [V_{M1}]
5-4	0 [0]	0 [0]	V_{M1} [0]	0 [V_{M1}]	dV_x [0]	0 [dV_x]	V_{M2} [V_{M1}]	V_{M1} [V_{M2}]
6-5	0 [0]	0 [0]	dV_x [0]	0 [dV_x]	dV_x [0]	0 [dV_x]	0 [V_{M2}]	V_{M2} [0]
7-6	0 [0]	0 [0]	dV_x [0]	0 [dV_x]	dV_x [0]	0 [dV_x]	V_{M1} [0]	0 [V_{M1}]
8-7	V_{M1} [0]	0 [V_{M1}]	dV_x [0]	0 [dV_x]	dV_x [0]	0 [dV_x]	V_{M2} [V_{M1}]	V_{M1} [V_{M2}]
9	dV_x [0]	0 [dV_x]	dV_x [0]	0 [dV_x]	dV_x [0]	0 [dV_x]	0 [V_{M2}]	V_{M2} [0]
10	dV_x [0]	0 [dV_x]	dV_x [0]	0 [dV_x]	dV_x [0]	0 [dV_x]	V_{M1} [0]	0 [V_{M1}]
9	dV_x [0]	0 [dV_x]	dV_x [0]	0 [dV_x]	dV_x [0]	0 [dV_x]	0 [V_{M2}]	V_{M2} [0]
8-9	dV_x [0]	0 [dV_x]	dV_x [0]	0 [dV_x]	V_{M1} [0]	0 [V_{M1}]	V_{M2} [V_{M1}]	V_{M1} [V_{M2}]
7-8	dV_x [0]	0 [dV_x]	dV_x [0]	0 [dV_x]	0 [0]	0 [0]	V_{M1} [0]	0 [V_{M1}]
6-7	dV_x [0]	0 [dV_x]	dV_x [0]	0 [dV_x]	0 [0]	0 [0]	0 [V_{M2}]	V_{M2} [0]
5-6	dV_x [0]	0 [dV_x]	V_{M1} [0]	0 [V_{M1}]	0 [0]	0 [0]	V_{M2} [V_{M1}]	V_{M1} [V_{M2}]
4-5	dV_x [0]	0 [dV_x]	0 [0]	0 [0]	0 [0]	0 [0]	V_{M1} [0]	0 [V_{M1}]
3-4	dV_x [0]	0 [dV_x]	0 [0]	0 [0]	0 [0]	0 [0]	0 [V_{M2}]	V_{M2} [0]
2-3	V_{M1} [0]	0 [V_{M1}]	0 [0]	0 [0]	0 [0]	0 [0]	V_{M2} [V_{M1}]	V_{M1} [V_{M2}]
1	0 [0]	0 [0]	0 [0]	0 [0]	0 [0]	0 [0]	V_{M1} [0]	0 [V_{M1}]

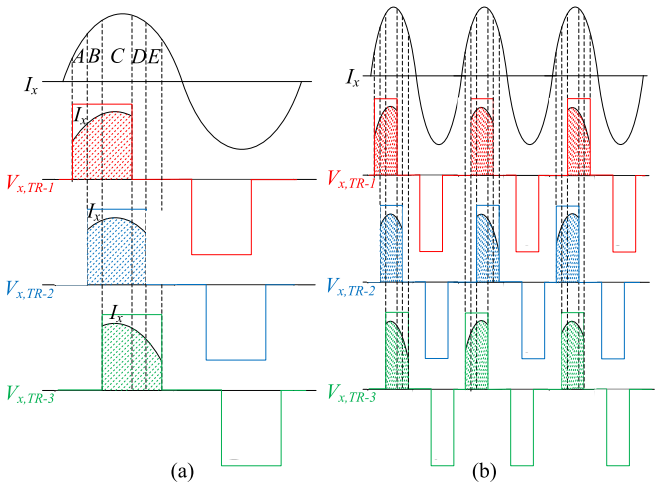

Fig. 4. Transmitted power of the MHBCs. (a) Applying a balanced voltage distribution. (b) With the MHBC rotating method.

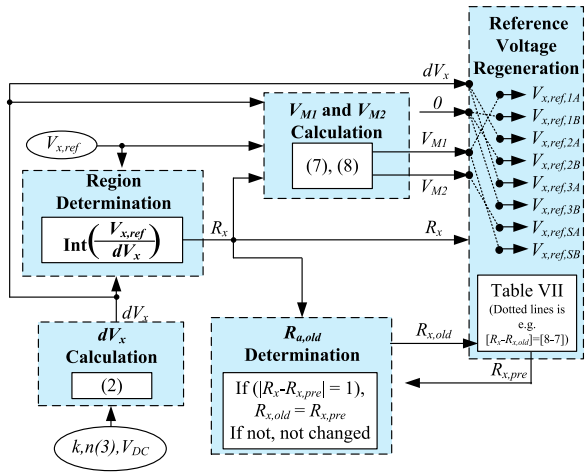

Fig. 5. Block diagram of the switching method for the transformer-based 21-level CHBI.

Fig. 5 shows the block diagram of the switching method for the transformer-based 21-level CHBI. The magnitude of the feasible maximum output voltage $(V_{x,\max})$ should be limited and using the parameters (V_{DC}, N, n, and k,) of the transformer-based CHBI topology's configuration, it is calculated as

$$V_{x,\max} = \frac{V_{\mathrm{DC}}}{k}N + \frac{V_{\mathrm{DC}}}{kn} \geq |V_{x,\mathrm{ref}}|. \tag{9}$$

E. Current Rate of the Transformer and Switching Devices

The voltage rate of the switching device depends on only the dc-link voltage connected to the HBC. The current rate of the transformer and switching devices is determined by the turn ratio and mutual inductance of the transformer, and the rated load current. The secondary side current $(I_{\mathrm{TR,sec}})$ of the transformer is the same as the load current (I_x). On the other hand, the primary side current $(I_{\mathrm{TR,pri}})$ is determined by two components: the active current $(I_{\mathrm{TR,act}})$ generated by $I_{\mathrm{TR,sec}}$ and the reactive current $(I_{\mathrm{TR,react}})$ caused by the mutual inductance (L_m) of the transformer. $I_{\mathrm{TR,act}}$ is calculated by $I_{\mathrm{TR,sec}}$, k and n of the transformer and it is expressed as

$$I_{\mathrm{TR,act}} = \frac{n}{k}I_{\mathrm{TR,sec}}. \tag{10}$$

$I_{\mathrm{TR,react}}$ is generated by L_m of the transformer and the output voltage ($V_{x,M}$ or $V_{x,\mathrm{Sub}}$) of HBC. Fig. 6 shows $V_{x,M}$ and $I_{\mathrm{TR,react}}$ when the load is not connected. It means that $I_{\mathrm{TR,sec}}$ is zero and $I_{\mathrm{TR,pri}}$ consists of only $I_{\mathrm{TR,react}}$. The slope of $I_{\mathrm{TR,react}}$ is $1/L_m$ and the peak value $(I_{\mathrm{TR,react,peak}})$ of

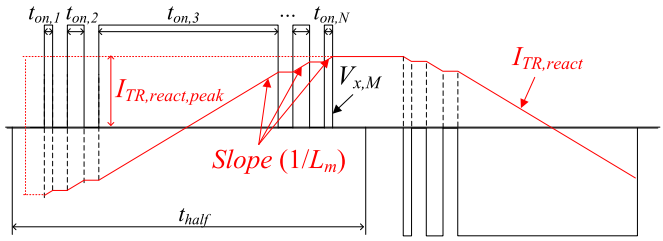

Fig. 6. Relationship between the output voltage $(V_{x,M})$ of HBC and the reactive current $(I_{\mathrm{TR,react}})$ at primary side of the transformer.

$I_{\mathrm{TR,react}}$ is calculated as

$$I_{\mathrm{TR,react,peak}} = \frac{1}{L}\int_0^{t_{\mathrm{half}}} V_{x,M}(t)dt = \frac{1}{L}\int_0^{t_{\mathrm{on,sum}}} V_{x,M,\mathrm{Mag}}dt \tag{11}$$

where t_{half} is the half time of the fundamental period of $V_{x,M}$ and $V_{x,M,\mathrm{Mag}}$ is the magnitude of $V_{x,M}$. The sum $(t_{\mathrm{on,sum}})$ of on-times $(t_{\mathrm{on},M}\ M = 1,\ldots,N)$ shown in Fig. 6 is expressed as

$$t_{\mathrm{on,sum}} = \sum_{M=1}^{N} t_{\mathrm{on},M}. \tag{12}$$

Consequently, $I_{\mathrm{TR,pri}}$ is determined by (10) and (11). They do not have the same phase and there is the phase difference of $\pi/2$ between $I_{\mathrm{TR,react}}$ and $I_{\mathrm{TR,act}}$. Although $I_{\mathrm{TR,react}}$ is not the sinusoidal waveform completely, $I_{\mathrm{TR,pri}}$ is expressed approximately as

$$I_{\mathrm{TR,pri}} = \sqrt{I_{\mathrm{TR,act}}^2 + I_{\mathrm{TR,react}}^2}. \tag{13}$$

As mentioned above, $I_{\mathrm{TR,pri}}$ can be considered to decide the switching device since it flows through the switching device.

If L_m of the transformer is large, $I_{\mathrm{TR,react}}$ can be reduced. It leads the current rate of the switching device to be decreased; however, the size and weight of the transformer increase to archive the large L_m. Consequently, there is tradeoff relationship of the rate current of switching device and the size and weight of the transformer. It will be considered in the design process of this system to optimize the cost-effective design solution.

In addition, the winding resistance $(R_{\mathrm{copper},x}, \mathrm{x} = \mathrm{pri, sec})$ and the leakage inductance $(L_{lk,x}, \mathrm{x} = \mathrm{pri, sec})$ of the transformer should be considered because the large $R_{\mathrm{copper},x}$ and $L_{lk,x}$ have the large voltage drop. It results in the distortion of V_a finally. Fig. 7 shows the equivalence circuit of the transformer. The voltage drops $(V_{\mathrm{drop},x}, \mathrm{x} = \mathrm{pri, sec})$ can be generated by four elements $(R_{\mathrm{copper,pri}}, R_{\mathrm{copper,sec}}, L_{lk,\mathrm{pri}}, L_{lk,\mathrm{sec}})$. Furthermore, they are main elements leading the loss of the transformer [29], [30]. Therefore, the small $R_{\mathrm{copper},x}$ and $L_{lk,x}$ of the transformer are required in the transformer-based CHBI topology.

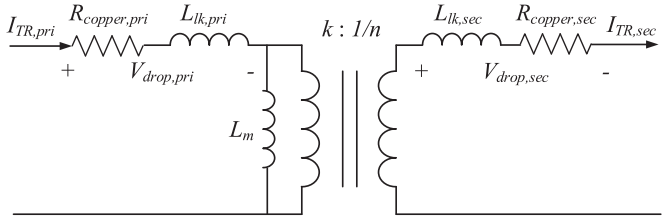

Fig. 7. Equivalence circuit of the transformer.

TABLE VIII
PARAMETERS AND OPERATING CONDITIONS

DC link voltage	100 V	DC link capacitor	2.64 mF
$V_{x,max}$	42 V_{peak}/50 Hz	f_{sw}	10 kHz
Control period	200 us	L_m of transformer	3.4 H

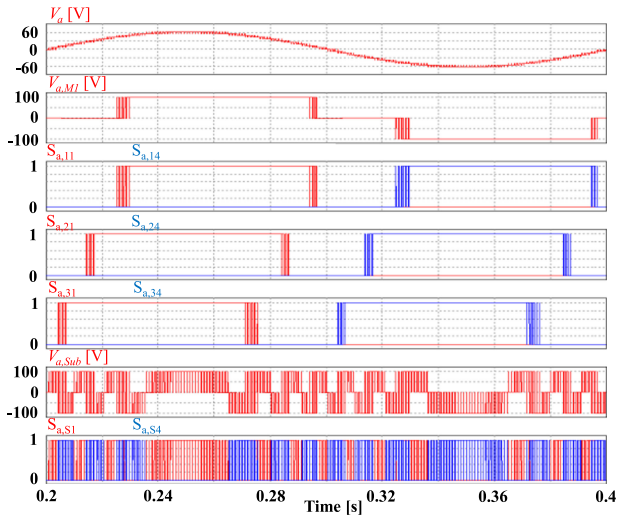

Fig. 8. Simulation results of the proposed switching method with the balanced voltage distribution at $M_i = 1$.

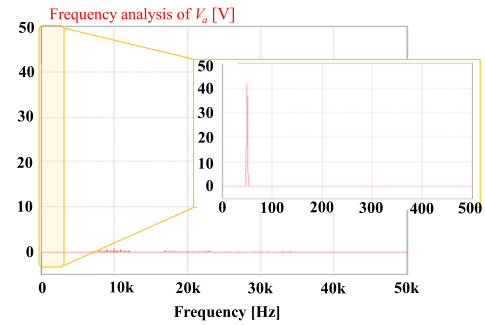

Fig. 9. Frequency analysis of the output voltage (V_a) of Fig. 8.

IV. SIMULATION RESULTS

The feasibility of the transformer-based CHBI topology is shown in this chapter. The configuration of the 21-level CHBI was considered for simulation and experiment. It is a three-phase system with four HBCs and four transformers in a phase. The operating conditions are listed in Table VIII and the parameters of the system are as follows: $N(4), n(3)$, and $k(8)$.

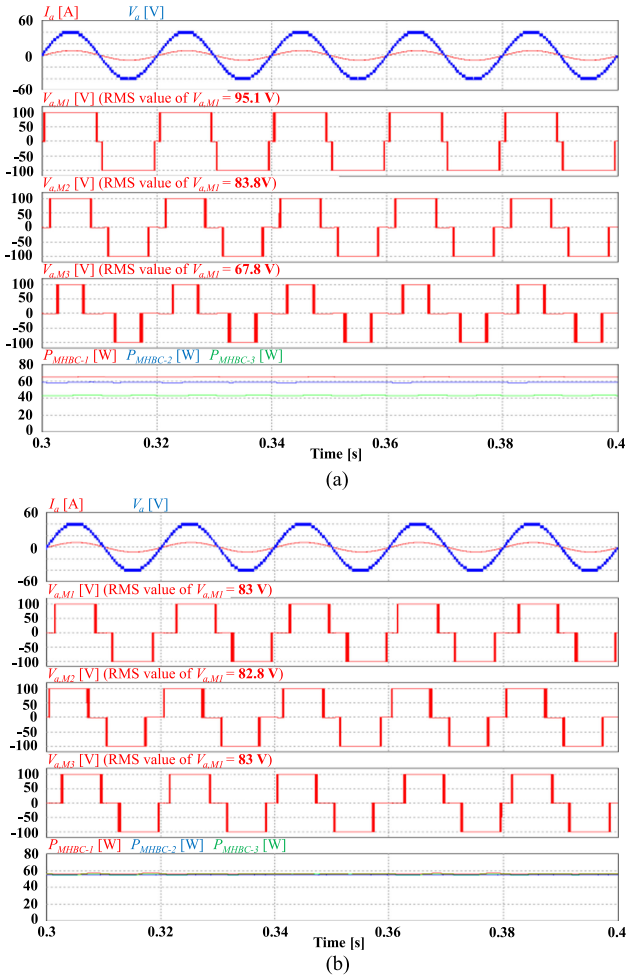

Fig. 10. Simulation results of the proposed switching method at $M_i = 1$. (a) With and (b) without the balanced voltage and power distributions.

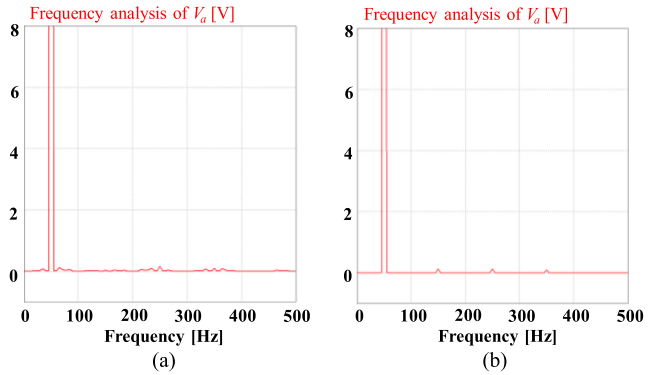

Fig. 11. Frequency analysis of the output voltage (V_a) at $M_i = 1$. (a) 10% turns ratio decrement of only TR-1. (b) 10% turns ratio decrement of only TR-Sub.

In the simulation and experiment, a modulation index (M_i) value is used and is expressed as

$$M_i = |V_{x,\mathrm{ref}}|_{\mathrm{mag}} / V_{x,\max}, x = a, b, c \tag{14}$$

where $|V_{x,\mathrm{ref}}|_{\mathrm{mag}}$ is the magnitude of $V_{x,\mathrm{ref}}$.

Fig. 8 shows the switching signals of a phase when the proposed switching method with the balanced voltage distribution

TABLE IX
TRANSFORMER PARAMETERS

Main transformer (TR-x, x=1,2,3)		Sub transformer (TR-sub)	
L_m	8.51 H	L_m	8.74 H
$L_{lk,pri}$	16.7 mH	$L_{lk,pri}$	19.2 mH
$R_{cooper,pri}$	4.27 Ω	$R_{cooper,pri}$	4.17 Ω
$L_{lk,sec}$	0.22 mH	$L_{lk,sec}$	0.50 mH
$R_{cooper,sec}$	0.14 Ω	$R_{cooper,sec}$	0.08 Ω

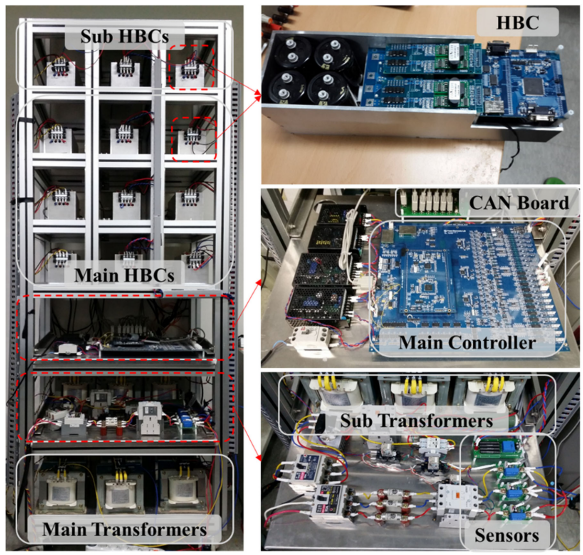

Fig. 12. Experimental setup of the transformer-based 21-level CHBI.

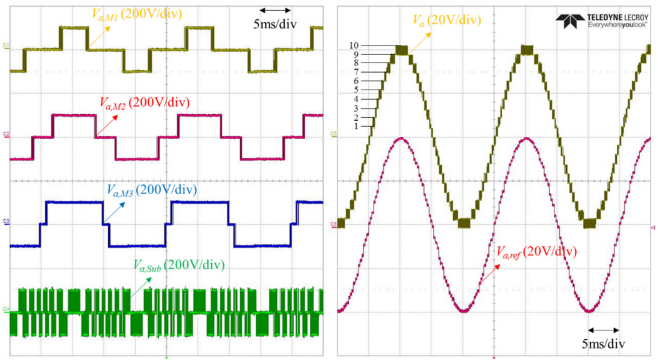

Fig. 13. Experimental results of the proposed switching method without a balanced voltage distribution at $M_i = 0.95$.

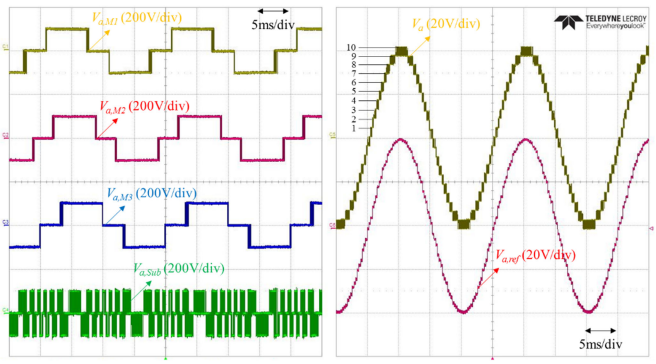

Fig. 14. Experimental results of the proposed switching method with a balanced voltage distribution at $M_i = 0.95$.

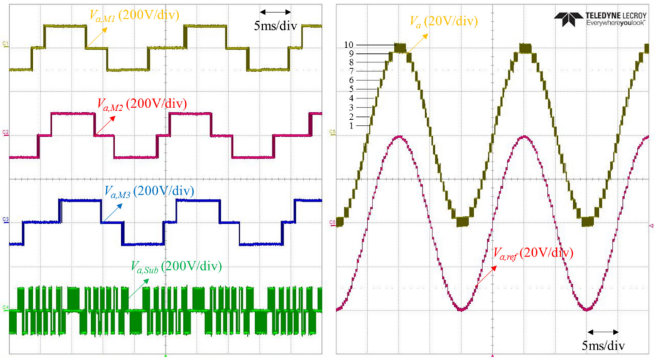

Fig. 15. Experimental results of the proposed switching method with balanced voltage and power distributions at $M_i = 0.95$.

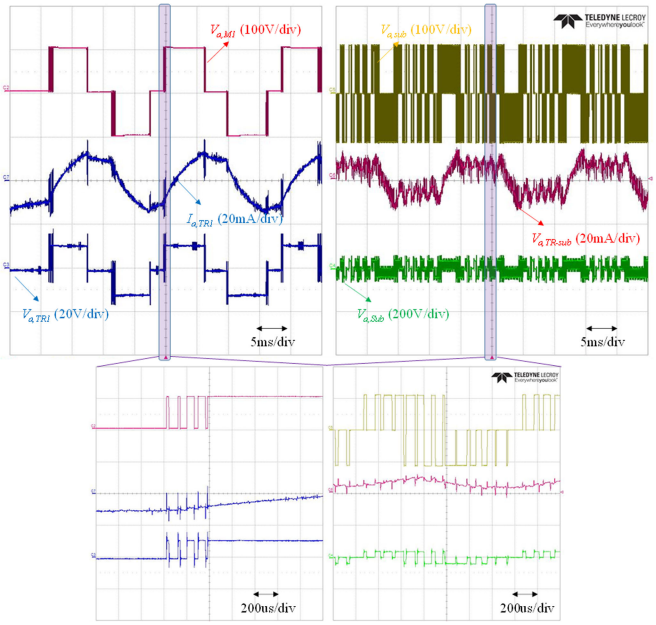

Fig. 16. Input $(V_{a,M1}, V_{a,\mathrm{sub}})$ and output $(V_{a,\mathrm{TR1}}, V_{a,\mathrm{TR-sub}})$ voltages of the transformer when the proposed switching method is applied.

TABLE X
POWER DISTRIBUTION RATIOS ($\mathrm{R} = 5\,\Omega$ AND $\mathrm{L} = 1$ MH)

	HBC-1	HBC-2	HBC-3
Case of Fig. 13	0.67	0.90	1
Case of Fig. 14	0.94	1	0.90
Case of Fig. 15	1	1	1

is applied. The shapes of the switching signals ($S_{a,y1}$ and $S_{a,y4}$, y is the cell number 1, 2, 3) for three MHBCs are almost similar to each other. As mentioned above, $S_{a,y1}$ and $S_{a,y2}$ ($S_{a,y3}$ and $S_{a,y4}$) are switched complementarily. The switching signals ($S_{a,S1}$ and $S_{a,S4}$) for SHBC are not the same as those of MHBC. It is because the proposed switching method applies the different switching scheme to SHBC to divide the output voltage into more levels. The frequency analysis of the output voltage (V_a) of Fig. 8 is shown in Fig. 9. We can see the switching frequency components (high frequency components) located near 10 kHz

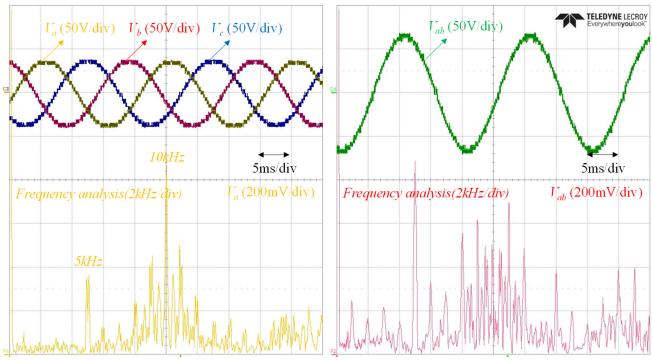

Fig. 17. Frequency spectrum of V_a and V_{ab} of the transformer-based CHBI topology with proposed switching method when $M_i = 1$.

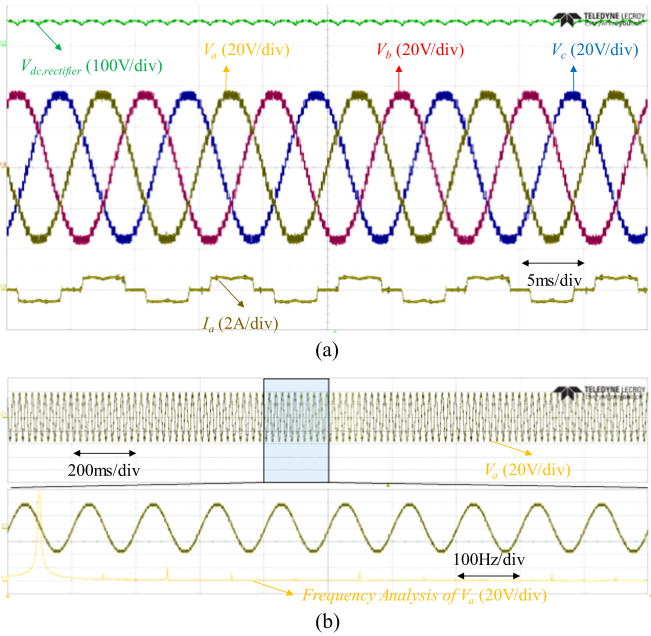

Fig. 18. Waveforms when the diode rectifier with R_{rec} (100 Ω) is connected to outputs of the transformer-based CHBI topology at $M_i = 1$.

which is the switching frequency of all HBCs have the small magnitude. In addition, there are no low frequency components in Fig. 9.

Fig. 10 shows the performance of the balanced voltage and power distributions contained in the proposed switching method. When the balanced voltage and power distributions are not applied as shown in Fig. 10(a), the output voltage's root mean square (rms) values of MHBCs are 95.1 V, 83.8 V, and 67.8 V, respectively. The powers delivered from MHBCs are not same. However, the balanced voltage and power distributions make the voltages and powers of MHBCs equal, respectively, as shown in Fig. 10(b).

The effect depending on the turns ratios variation of the transformer is analyzed. In the normal state, one frequency component which is the fundamental frequency component is shown in the low frequency range (0 to 500 Hz) of Fig. 9. However, the turns ratios variation of the transformer generates the other frequency components in V_a. The 10% turn ratios variation of

TABLE XI
COMPARISON ANALYSIS OF THE TOPOLOGY USED IN THIS PAPER AND OTHER TOPOLOGIES (21-LEVEL OF OUTPUT VOLTAGE IN SINGLE PHASE)

	The transformer-based CHBI (21-level)	The conventional CHBI (21-level)	The neutral-point clamped inverter
H-bridge (Device)	4 (IGBT: 16)	10(IGBT: 40)	-(IGBT: 40, Diode: 180)
Single phase TR	4 (two types)	10 (one type)	1
Rectifier	1	10	1
PWM Scheme	Two PWM schemes (one for MHBCs/one for SHBC)	One PWM scheme in all HBCs	One PWM scheme in the inverter
Operating mode	Three MHBCs in the same operation mode and a SHBC in the unique operation mode	All (ten) HBCs in the same operation mode	One operation mode in the inverter

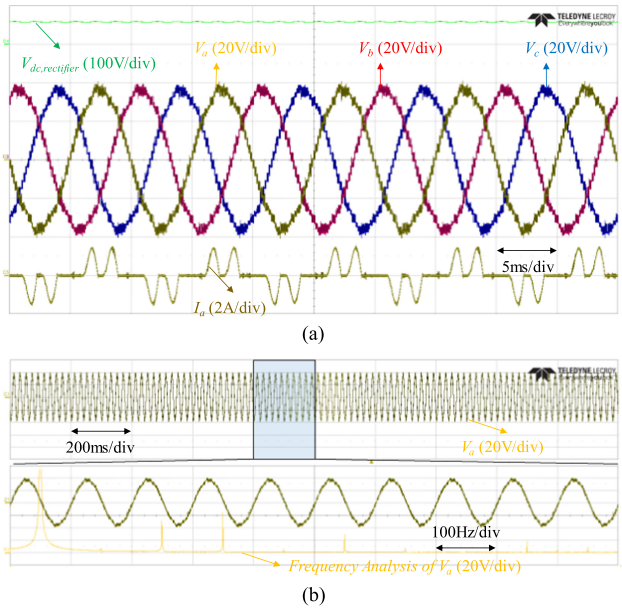

Fig. 19. Waveforms when the diode rectifier with $R_{\rm rec}$ (100 Ω) and $C_{\rm rec}$ (330 μF) is connected to outputs of the transformer-based CHBI topology at $M_i = 1$.

one transformer is considered and these results are shown in Fig. 11.

V. EXPERIMENTAL RESULTS

The feasibility of the transformer-based CHBI topology with the proposed switching method was verified experimentally. The experimental parameters are the same as those of simulation, but the transformer parameters are shown in Table IX. The experimental setup is shown in Fig. 12. The same HBC is used for the MHBC and SHBC and each HBC has a subcontroller, TMS320F28335. TMS320C28346 was used as the main controller. It calculates the reference voltages $(V_{x,{\rm ref},yA}, V_{a,{\rm ref},yB}, x = a, b, c, y = 1, 2, 3, S)$ for all the HBCs and these are transmitted to the subcontroller through CAN communication (data rate: 1 Mb/s) with the synchronization signal for the PWM operations. In the subcontroller, switching signals are generated by a switching function internally installed. The dc source (Chroma, 62959H-600), the oscilloscope (Lecroy, HDO8108), and voltage (Lecroy, AP031) and current (Lecroy, AP015) probes are used for the measurements in the experiment.

Fig. 13 shows the experimental results of the transformer-based CHBI topology applying the proposed switching method without a balanced voltage distribution. Although V_a with a high voltage level generates, the output voltages $(V_{a,M1}, V_{a,M2}, V_{a,M3})$ of the HBCs have different clamping durations.

Fig. 14 shows the experimental results of proposed switching method with the balanced voltage distribution. $V_{a,M1}, V_{a,M2,}$ and $V_{a,M3}$ have the same shape and are synthesized as V_a that is the same as that of Fig. 13. In Fig. 15, a balanced power distribution is applied with a balanced voltage distribution. Although V_a is the same as that of Figs. 13 and 14, $V_{a,M1}, V_{a,M2}$, and $V_{a,M3}$ are not the same as those of them. The output voltages are rotated in every fundamental period and all the HBCs achieve a balanced power distribution as Table X.

The input $(V_{a,M1}, V_{a,{\rm sub}})$ and output $(V_{a,{\rm TR1}}, V_{a,{\rm TR-sub}})$ voltages of the transformer are shown in Fig. 16. The transformer input current $(I_{a,{\rm TR1}})$ in Fig. 16 depends upon the transformer design.

The frequency spectrum of V_a and V_{ab} of the transformer-based CHBI topology is shown in Fig. 17. The magnitude of the fundamental frequency component (50 Hz) is 41.66 when $M_i = 1$. The switching frequency components (around 10 kHz) have a small magnitude under 1 V. Similar to the case of V_a, the switching frequency components of the line-to-line voltage (V_{ab}) have a small magnitude. The 5 kHz component in Fig. 17 is caused by the control period.

The experimental results are shown in Figs. 18 and 19 when the three-phase diode rectifier is connected to outputs of the transformer-based CHBI topology with the proposed switching method. In Fig. 18, only resistor $(R_{\rm rec}, 100\,\Omega)$ is connected on the dc side of the diode rectifier. Since the capacitor does not exist at dc side of the diode rectifier, the dc-side voltage $(V_{\rm dc,rectifier})$ has the low frequency component which is six times the fundamental frequency of V_a. In addition, V_a has the several frequency components as shown in the frequency analysis and they are the voltage distortion of V_a. The capacitor ($C_{\rm rec}$, 330 μF) is connected to the dc side of the diode rectifier additionally in Fig. 19. In this case, the voltage distortion of V_a increases more than Fig. 18. It is because the current (I_a) of Fig. 19 contains the harmonic frequency components more than that of Fig. 18. Based on analysis of the chapter III-E and results of Figs. 18 and 19, we can know that the voltage distortion is generated not by the proposed switching method but by the transformer characteristic.

VI. Conclusion

Transformer-based CHBI topology was introduced in this paper. The comparison analysis between topologies was shown in Table XI. The theoretical analysis regarding the selection of the turns ratio of the subtransformer was presented. In addition, a switching method based on the level-shifted switching method with the balanced voltage and power distributions was proposed for the transformer-based CHBI topology. Several requirements related to the decision of switching devices and the design of transformer were suggested. A 21-level CHBI was used to determine the feasibility and effectiveness of the proposed switching method.

When using the proposed switching method, two issues are to be noted: 1) to use the proposed switching method, the configuration of transformer-based CHBI topology should follow that of Table II. It guarantees that the minimum variation (dV_x) of the voltage level is always the same. 2) If the system operates in the wide voltage range (wide M_i), Table VII should be changed as that explained in this paper to guarantee a balanced voltage distribution for M_i range required. Table VI guarantees a balanced voltage distribution for $0.8 < M_i < 1$. Consequently, this configuration can be applied for the main power supply system generating the ac voltage in grid.

References

[1] J. Rodríguez, S. Bernet, B. Wu, J. O. Pontt, and S. Kouro, "Multilevel voltage-source-converter topologies for industrial medium-voltage drives," *IEEE Trans. Ind. Electron.*, vol. 54, no. 6, pp. 2930–2945, Dec. 2007.

[2] J. S. Lee and K. B. Lee, "New modulation techniques for a leakage current reduction and a neutral-point voltage balance in transformerless photovoltaic systems using a three-level inverter," *IEEE Trans. Power Electron.*, vol. 29, no. 4, pp. 1720–1732, Apr. 2014.

[3] C. H. Ng, M. A. Parker, L. Ran, P. J. Tavner, J. R. Bumby, and E. Spooner, "A multilevel modular converter for a large, light weight wind turbine generator," *IEEE Trans. Power Electron.*, vol. 23, no. 3, pp. 1062–1074, May 2008.

[4] V. Yaramasu and B. Wu, "Predictive control of a three-level boost converter and an NPC inverter for high-power PMSG-based medium voltage wind energy conversion systems," *IEEE Trans. Power Electron.*, vol. 29, no. 10, pp. 5308–5322, Oct. 2014.

[5] J. Mei, B. Xiao, K. Shen, L. M. Tolbert, and J. Y. Zheng, "Modular multilevel inverter with new modulation method and its application to photovoltaic grid-connected generator," *IEEE Trans. Power Electron.*, vol. 28, no. 11, pp. 5063–5073, Nov. 2013.

[6] L. Wang, D. Zhang, Y. Wang, B. Wu, and H. S. Athab, "Power and voltage balance control of a novel three-phase solid-state transformer using multilevel cascaded H-bridge inverters for microgrid applications," *IEEE Trans. Power Electron.*, vol. 31, no. 4, pp. 3289–3302, Apr. 2016.

[7] M. Z. Youssef, K. Woronowicz, K. Aditya, N. A. Azeez, and S. S. Williamson, "Design and development of an efficient multilevel DC/AC traction inverter for railway transportation electrification," *IEEE Trans. Power Electron.*, vol. 31, no. 4, pp. 3036–3042, Apr. 2016.

[8] M. Hagiwara, K. Nishimura, and H. Akagi, "A medium-voltage motor drive with a modular multilevel PWM inverter," *IEEE Trans. Power Electron.*, vol. 25, no. 7, pp. 1786–1799, Jul. 2010.

[9] J. Mathew, K. Mathew, N. A. Azeez, P. P. Rajeevan, and K. Gopakumar, "A hybrid multilevel inverter system based on dodecagonal space vectors for medium voltage IM drives," *IEEE Trans. Power Electron.*, vol. 28, no. 8, pp. 3723–3732, Aug. 2013.

[10] J. Huang and K. A. Corzine, "Extended operation of flying capacitor multilevel inverters," *IEEE Trans. Power Electron.*, vol. 21, no. 1, pp. 140–147, Jan. 2006.

[11] J. Amini, "An effortless space-vector-based modulation for N-level flying capacitor multilevel inverter with capacitor voltage balancing capability," *IEEE Trans. Power Electron.*, vol. 29, no. 11, pp. 6188–6195, Nov. 2014.

[12] N. A. Rahim, M. F. M. Elias, and W. P. Hew, "Transistor-clamped H-bridge based cascaded multilevel inverter with new method of capacitor voltage balancing," *IEEE Trans. Ind. Electron.*, vol. 60, no. 8, pp. 2943–2956, Aug. 2013.

[13] M. Abolhassani, "Modular multipulse rectifier transformers in symmetrical cascaded H-bridge medium voltage drives," *IEEE Trans. Power Electron.*, vol. 27, no. 2, pp. 698–705, Feb. 2012.

[14] K. M. Tsang and W. L. Chan, "Single DC source three-phase multilevel inverter using reduced number of switches," *IET Power Electron.*, vol. 7, no. 4, pp. 775–783, Apr. 2014.

[15] A. Taghvaie, J. Adabi, and M. Rezanejad, "Circuit topology and operation of a step-up multilevel inverter with a single DC source," *IEEE Trans. Ind. Electron.*, vol. 63, no. 11, pp. 6643–6652, Nov. 2016.

[16] A. Rahul S, S. Pramanick, M. Boby, K. Gopakumar, and L. G. Franquelo, "Extended linear modulation operation of a common-mode-voltage-eliminated cascaded multilevel inverter with a single DC supply," *IEEE Trans. Ind. Electron.*, vol. 63, no. 12, pp. 7372–7380, Dec. 2017.

[17] A. K. Panda and Y. Suresh, "Performance of cascaded multilevel inverter by employing single and three-phase transformers," *IET Power Electron.*, vol. 5, no. 9, pp. 1694–1705, Nov. 2015.

[18] S. G. Song, F. S. Kang, and S. J. Park, "Cascaded multilevel inverter employing three-phase transformers and single DC input," *IEEE Trans. Ind. Electron.*, vol. 56, no. 6, pp. 2005–2015, Jun. 2009.

[19] M. R. Banaei, H. Khounjahan, and E. Salary, "Single-source cascaded transformers multilevel inverter with reduced number of switches," *IET Power Electron.*, vol. 5. no. 9, pp. 1748–1753, Sep. 2012.

[20] F. S. Kang, S. J. Park, M. H. Lee, and C. U Kim, "An efficient multilevel-synthesis approach and its application to a 27-level inverter," *IEEE Trans. Ind. Electron.*, vol. 52, no. 6, pp. 1600–1606, Dec. 2005.

[21] B. Wu, *High-Power Converters and AC Drives*. Hoboken, NJ, USA: Wiley, 2006.

[22] H. W. Sim, J. S. Lee, and K. B. Lee, "Detecting open-switch faults: Using asymmetric zero-voltage switching states," *IEEE Ind. Appl. Mag.*, vol. 22, no. 2, pp. 27–37, Mar./Apr. 2016.

[23] E. da Silva, E. Dos Santos, and C. Jacobina, "Pulsewidth modulation strategies," *IEEE Ind. Electron. Mag.*, vol. 5, no. 2, pp. 37–45, Jun. 2011.

[24] U. M. Choi, F. Blaabjerg, and K. B. Lee, "Study and handling methods of power IGBT module failures in power electronic converter systems," *IEEE Trans. Power Electron.*, vol. 30, no. 5, pp. 2517–2533, May 2015.

[25] C. Busca *et al.*, "An overview of the reliability prediction related aspects of high power IGBTs in wind power applications," *Microelectron. Rel.*, vol. 51, no. 9–11, pp. 1903–1907, Sep./Nov. 2011.

[26] S. M. Kim, J. S. Lee, and K. B. Lee, "A modified level-shifted PWM strategy for fault tolerant cascaded multilevel inverters with improved power distribution," *IEEE Trans. Ind. Electron.*, vol. 66, no. 11, pp. 7264–7274, Nov. 2016.

[27] L. M. Tolbert, F. Z. Peng, and T. G. Habetler, "Multilevel PWM methods at low modulation indices," *IEEE Trans. Power Electron.*, vol. 15, no. 4, pp. 719–725, Jul. 2000.

[28] R. T. H. Li, H. S. H. Chung, W. H. Lau, and B. Zhou, "Use of hybrid PWM and passive resonant snubber for a grid-connected CSI," *IEEE Trans. Power Electron.*, vol. 25, no. 2, pp. 298–309, Feb. 2010.

[29] Y. Han, W. Eberle, and Y. F. Liu, "A practical copper loss measurement method for the planar transformer in high-frequency switching converters," *IEEE Trans. Ind. Electron.*, vol. 54, no. 4, pp. 2276–2287, Aug. 2007.

[30] P. Huang *et al.*, "Optimal design and implementation of high-voltage high-power silicon steel core medium-frequency transformer," *IEEE Trans. Ind. Electron.*, vol. 64, no. 6, pp. 4391–4401, Jun. 2017.

June-Seok Lee (S'11–M'15) received the B.S., M.S., and Ph.D. degrees in electrical and computer engineering from Ajou University, Suwon, South Korea, in 2011, 2013, and 2015, respectively.

Since 2015, he has been with the Korea Railroad Research Institute, Uiwang, Korea. His research interests include high power electric machine drives, grid-connected systems, multilevel inverters, and reliability.

Hyun-Woo Sim received the B.S. and M.S. degrees in electrical and computer engineering from Ajou University, Suwon, South Korea, in 2013 and 2015, respectively.

He has been with the Hyundai Mobis, Yongin, South Korea, as a Research Engineer since 2015. His research interests include electric machine drives, multilevel inverters, and battery management systems.

Juyong Kim received the M.S. and Ph.D. degrees in electrical and electronic engineering degrees from Kyungpook National University, Daegu, South Korea, in 1994 and 2007, respectively.

He joined Korea Electric Power Research Institute, Naju, South Korea, in 1994. His current research interests include the design and control of dc distribution systems.

Kyo-Beum Lee (S'02–M'04–SM'10) received the B.S. and M.S. degrees in electrical and electronic engineering from the Ajou University, Suwon, South Korea, in 1997 and 1999, respectively. He received the Ph.D. degree in electrical engineering from Korea University, Seoul, South Korea, in 2003.

From 2003 to 2006, he was with the Institute of Energy Technology, Aalborg University, Aalborg, Denmark. From 2006 to 2007, he was with the Department of Electrical Engineering, Chonbuk National University, Jeonju, South Korea. In 2007, he joined the Department of Electrical and Computer Engineering, Ajou University. His research interests include electric machine drives, renewable power generation, and electric vehicle applications.